ELSEVIER

Contents lists available at ScienceDirect

Molecular Catalysis

journal homepage: www.journals.elsevier.com/molecular-catalysis





CuNi bimetallic nanocatalyst enables sustainable direct carboxylation reactions

Neha Choudhary ^a, Mona Abdelgaid ^b, Giannis Mpourmpakis ^b, Shaikh M. Mobin ^{a,c,d,*}

- a Department of Chemistry, Indian Institute of Technology-Indore, Khandwa road, Simrol 433552, India
- b Department of Chemical and Petroleum Engineering, University of Pittsburgh, Pittsburgh, Pennsylvania 15261, United States
- ^c Department of Biosciences and Bio-Medical Engineering, Indian Institute of Technology-Indore, Khandwa road, Simrol 433552, India
- d Center for Electric Vehicle and Intelligent Transport Systems, Indian Institute of Technology-Indore, Khandwa road, Simrol 433552, India

ARTICLE INFO

Keywords: Carboxylation reaction Bimetallic nanocatalyst Recyclable catalyst Solvent-free reaction

ABSTRACT

Herein, we combine catalyst synthesis, characterization, catalytic experiments, and theory to investigate the bimetallic CuNi-11 nanocatalyst for direct carboxylation of arenes. Catalytic experiments reveal that the CuNi-11 shows an excellent yield and a higher benzene conversion compared to monometallic Cu and Ni nanocatalysts. The bimetallic CuNi-11 nanocatalyst exhibits a high surface area of $58.993~\text{m}^2/\text{g}$ with excellent reusability (up to 6 cycles) and the carboxylation reaction is an activator-, additive- and solvent-free taking place under mild conditions. Catalytic experiments are complemented by Density Functional Theory (DFT) calculations demonstrating a plausible mechanistic pathway involving C-H bond activation of benzene and formic acid. The benzoic acid and H_2 formation with the benzene C-H activation being the rate-determining step. Overall, our work contributes to introducing sustainable and environmentally friendly carboxylation routes of arenes with a new mechanistic approach.

Introduction

Heterogeneous catalysis has attracted tremendous attention in modern industry as it plays a vital role in the production of chemicals and pharmaceuticals. Heterogeneous catalysts offer many advantages over homogeneous catalysts including the high catalytic stability under reaction conditions and recyclability through the facile separation of the liquid or gaseous products from the solid catalyst. Among the different fields of heterogeneous catalysis, catalysis by transition metal nanoparticles is one of the most important, owing to their inherent properties that include variation of metal oxidation state, high surface energy which increases the activity of surface atoms, high surface-to-volume ratio, environmental abundance, and cost-effectiveness [1,2]. Hence, the use of transition metal nanoparticles as heterogeneous catalysts is an attractive alternative to homogeneous metal complexes [3]. Additionally, bimetallic nanoparticles have drawn a greater interest than monometallic nanoparticles due to the synergistic effects between individual metals present in the bimetallic system [4-6], leading to higher chemical activity and enhanced chemical, biological, and magnetic properties [7,8]. Specifically, magnetic bimetallic nanocatalysts show promise in heterogeneous catalysis owing to their ease of separation directly from the reaction mixture using an external magnet [9].

The transformation of C-C and C-H bonds has a major impact on the field of organic synthesis and pharmaceutical industry for the production of natural products and various crucial intermediates [10]. Specifically, aromatic carboxylic acids have found tremendous applications in the pharmaceutical and chemical industry [11,12]. For example, benzoic acid and its derivatives are commonly used as antimicrobial preservatives, flavouring agents, and food additives. Owing to their application, significant research efforts have been devoted to developing new synthetic protocols to produce these value-added synthons. One of the most promising approaches is the direct carboxylation of aromatic compounds to their corresponding aromatic acid analogues. However, the direct functionalization of aromatic non-activated C-H bonds remains a daunting task in synthetic and organometallic chemistry due to the high chemical stability and inert nature of the arenes C-H bonds [13].

However, the carboxylation of arenes proceeds via four major pathways: (i) base-mediated (i.e. Kolbe-Schmitt reaction type) [14] (ii) Lewis-acid-mediated (i.e. Friedel-Crafts reaction type) (iii) transition-metal catalyzed, and (iv) enzymatic carboxylation [15]. The base-mediated carboxylation involves the use of a base to avoid the

E-mail address: xray@iiti.ac.in (S.M. Mobin).

^{*} Corresponding author.

formation of undesired H₂O, however, high pressure of CO₂ is still required. The carboxylation via Lewis-acid mediated pathway involves the use of AlCl₃/Al with CO₂ gas which occurs on the most nucleophilic site of arenes [16]. Additionally, several studies have reported the C-H activation and carboxylation of aromatic compounds using monometallic catalysts, including Pd [17], Cu [18], Ni [19], Ir [20], Rh [21] which either involve the use of highly toxic CO or chemically stable CO₂ gases with oxidizing agents. Besides, some studies used N, N'-dicyclohexylcarbodiimide (DCC) as an additive with formic acid for the carboxylation reaction which required a catalytic amount of DCC and pre-activated substrate such as aryl halide instead of benzene, in addition to high reaction temperature [22]. Also, the existing procedure involves the use of non-recyclable, precious metal complexes as catalysts with high loadings, oxidants, or activators along with the high reaction temperature and time. Henceforth, the development of a recyclable, cost-effective heterogeneous catalyst for the carboxylation of arene via an activator-free, gas-free, and additive-free approach needs to be explored.

In this context, formic acid is a suitable carbonyl source, owed to its non-toxicity, accessible synthetic approaches, and cost-effectiveness due to its availability as a by-product from the industrial sector [23,24]. Also, formic acid can be used as an alternative to CO and CO₂ gases for the carboxylation of arenes [22,25]. Moreover, several computational studies have been reported so far to elucidate the catalytic activation and decomposition strategies of formic acid on monometallic transition metal surfaces, such as Pt [26] Cu, [27,28], Ni [29,30], Au [31,32], and Pd [30] and bimetallic transition surfaces such as PtPd[33] and PdCu [34,35]. These studies pave the path for the utilization of formic acid on copper and nickel metal surfaces for carboxylation reactions due to their low cost and high abundance [36,37] over expensive metals like Pd, Pt, Ru, Rh because the cost-effectiveness is an important factor for industry.

In this work, we utilize CuNi bimetallic nanocatalysts for the carboxylation of benzene in the presence of formic acid as carboxylating agent in solvent-free condition as a sustainable and environmentally benign approach [23,38,39]. Specifically, we combined catalytic experiments in conjunction with DFT calculations to report an easily synthesizable, magnetically recoverable CuNi-11 bimetallic nanocatalyst for the catalytic conversion of arenes utilizing formic acid, with an activator-free, gas-free and solvent-free approach.

Results and discussion

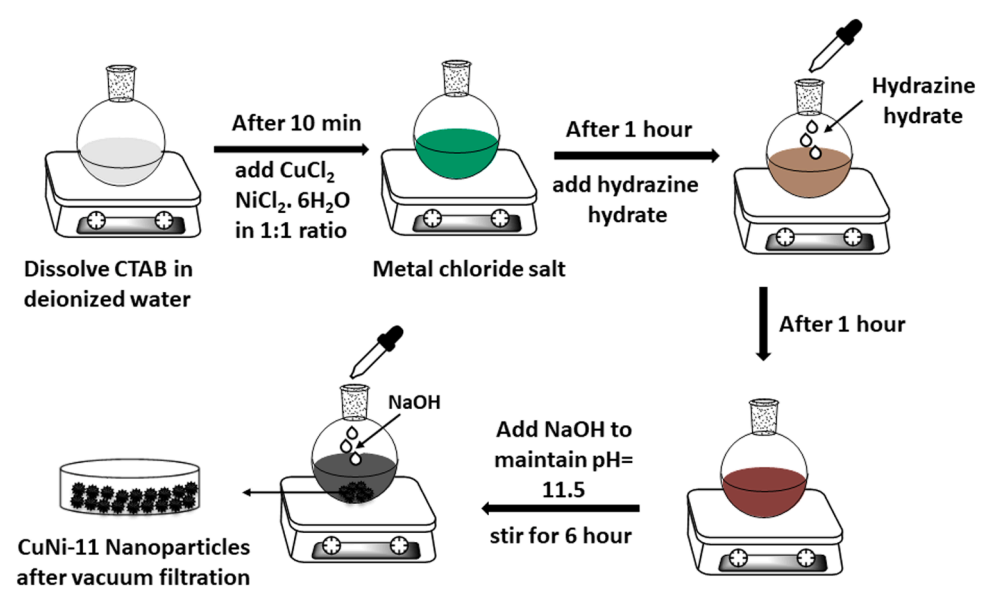
Characterization of bimetallic CuNi-11 nanocatalysts

The synthesis of all CuNi nanocatalysts was performed by varying the Cu:Ni molar ratios such as CuNi-11(1:1), CuNi-12(1:2), CuNi-21(2:1), and monometallic Cu and Ni were also considered (Scheme 1).

All the synthesized nanocatalysts including CuNi-11, CuNi-12, CuNi-21, monometallic Cu and monometallic Ni were synthesized and characterized by PXRD analysis (Figure S1). The PXRD analysis of CuNi-11 showed diffraction peaks at 19.05°, 33.22°, 38.34°, 58.94°, and 62.54° corresponding to (001), (100), (101), (110), and (111) planes, respectively, which imply the presence of β -Ni(OH)₂ (JCPDS #14-0117) as shown in Fig. 1A [40,41]. The diffraction peaks at 43.41°, 50.49°, and 74.16° corresponded to (111), (200), and (220) planes, respectively, which are attributed to Cu (JCPDS#04-0836) [42,43]. The PXRD patterns of the three bimetallic nanoparticles (CuNi-11, Cu-Ni-12, and CuNI-21) were compared with monometallic Cu and Ni nanoparticles (Figure S1), and the shifts in PXRD peaks suggested that the synthesized bimetallic nanoparticles are alloys and do not exhibit a core-shell geometry. The average crystallite size calculated by the Debye Scherrer equation was found to be 5 nm.

Furthermore, the FT-IR spectrum of bimetallic CuNi-11 nanocatalyst was performed (Figure S2) and the absorption peak at 3406 cm $^{-1}$ indicates the presence of CTAB for OH vibration of hydroxyl group [44, 45]. The peaks at 2918, 1716, and 1257 cm $^{-1}$ are attributed to C-H stretching bands of CTAB surfactant [46]. The absorption peaks at 1636 and 1496 cm $^{-1}$ are attributed to asymmetric and symmetric stretching vibrations of N $^+_{\rm CH_3}$ and 760 cm $^{-1}$ is assigned for Br $^-$ of CTAB [9]. The absorption peak at 455 cm $^{-1}$ is attributed to stretching vibration of metal-metal i.e. Cu-Ni band [46]. This data revealed the capping of CTAB on bimetallic CuNi-11 nanocatalyst.

Thermogravimetric analysis (TGA) was performed to check the thermal stability (Fig. 1B) under $\rm N_2$ atmosphere from 30°C to 800°C. There were two major weight losses observed in the region of (i) up to 250°C and (ii) above 250°C. The weight loss in these regions was observed at 8.29 wt% and 4.64 wt%, respectively. The first weight loss is due to the partial removal of adsorbed CTAB and water molecules [47, 48] or decomposition of CTAB which was attached to the surface of CuNi-11. The second weight loss was attributed to the complete oxidation of CTAB layer capping. These results indicate the high thermal stability of the synthesized bimetallic CuNi-11 nanocatalyst up to high



Scheme 1. Schematic representation of the synthesis of CuNi-11 nanocatalyst.

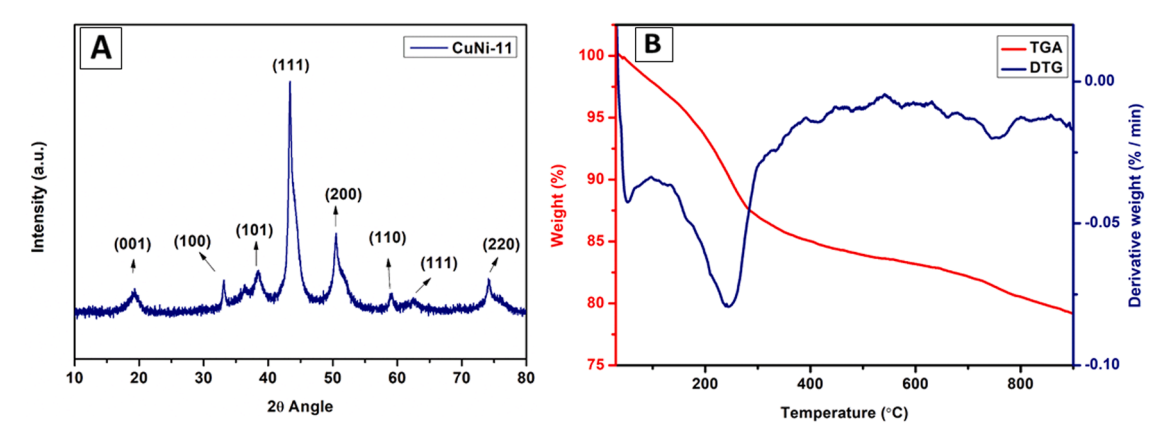


Fig. 1. (A) PXRD spectra and (B) thermogravimetric analysis of CuNi-11 nanocatalyst.

temperatures. For better clarification of weight loss with increasing the temperature, the differential derivative thermogravimetric analysis (DTG) was also added in Fig. 1B.

High surface area plays a key role to enhance the catalytic performance. Thus, to quantify the surface area of the synthesized bimetallic catalysts, the N_2 adsorption-desorption studies were performed by employing Brunauer-Emmett-Teller (BET) surface area analyzer at 77 K and 1 bar. The calculated specific surface area, pore size, and pore volume were found to be $58.993~\text{m}^2/\text{g}$, 7.76~nm, and $0.136~\text{cm}^2/\text{g}$, respectively (Fig. 2). The N_2 adsorption curve exhibited type IV isotherm with H3 hysteresis loop, indicating the presence of mesopores [49,50]. Moreover, CO_2 adsorption-desorption studies performed at 298~K and 1~bar revealed maximum CO_2 uptake of $95.546~\text{m}^2/\text{g}$. The results demonstrate that the CuNi-11 nanocatalyst is more selective towards

 CO_2 over N_2 , showing a potential for application of CuNi-11 nanocatalyst in CO_2 capture technologies [51,52].

Surface morphology plays an important role in the catalytic activity and selectivity [53,54] and for that, the surface morphological studies were performed using FE-SEM analysis of the CuNi-11 nanocatalyst. The overall morphology revealed nanoflakes type structures which were arranged in nanoflower-like shapes (Fig. 3(A-B)) [55,56]. Furthermore, the elemental analysis and mapping of CuNi-11 nanocatalyst confirmed the presence of Cu and Ni elements with a 1:1 wt% ratio (Fig. 3(C-E)). Furthermore, the detailed morphology of the synthesized bimetallic CuNi-11 nanocatalyst was analyzed using HR-TEM (Fig. 4(A-C)). The observed images were in accordance with FE-SEM imaging of nanoflakes-like structures. Additionally, the d-spacing was calculated from TEM images to be 0.27, 0.18, and 0.15 nm for (100), (110) planes

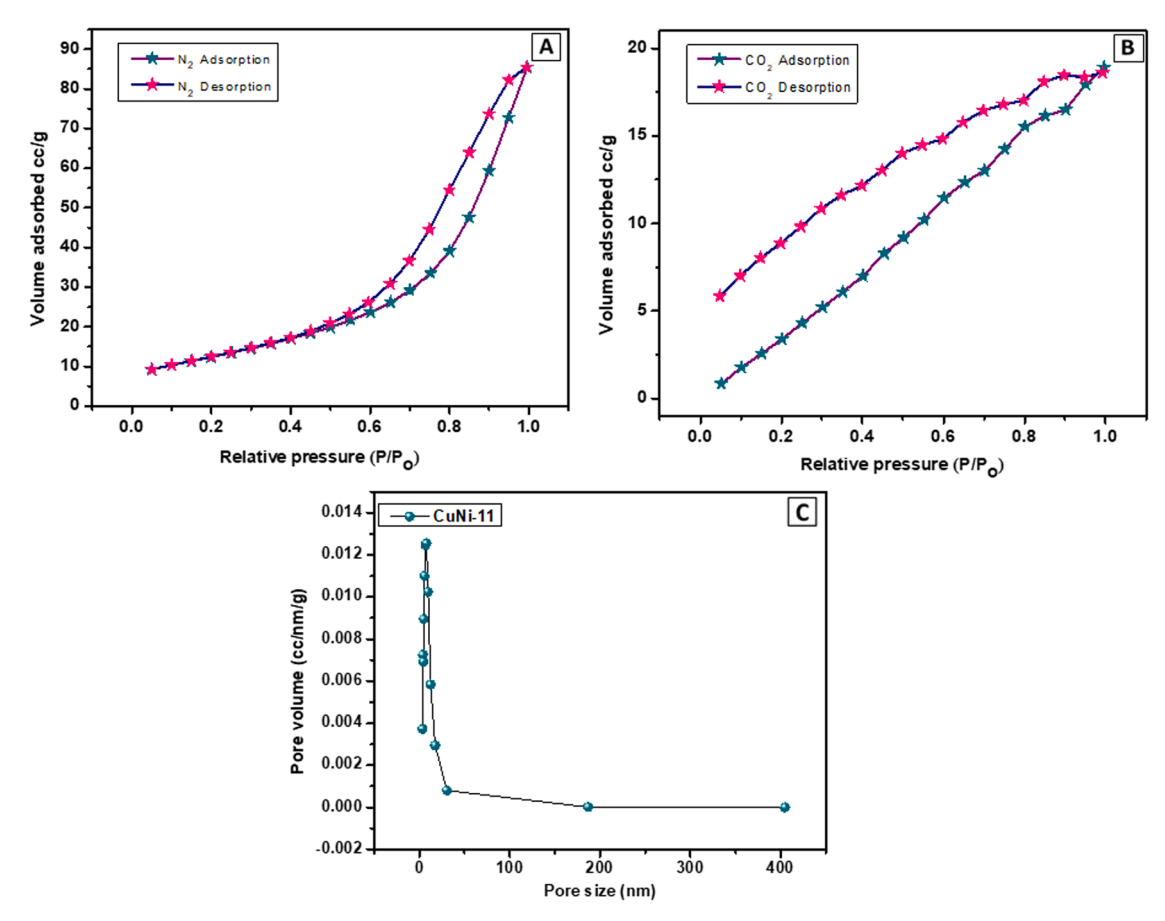


Fig. 2. (A) N₂ adsorption-desorption (B) CO₂ adsorption-desorption (C) BJH pore-size distribution isotherm of CuNi-11 nanocatalyst.

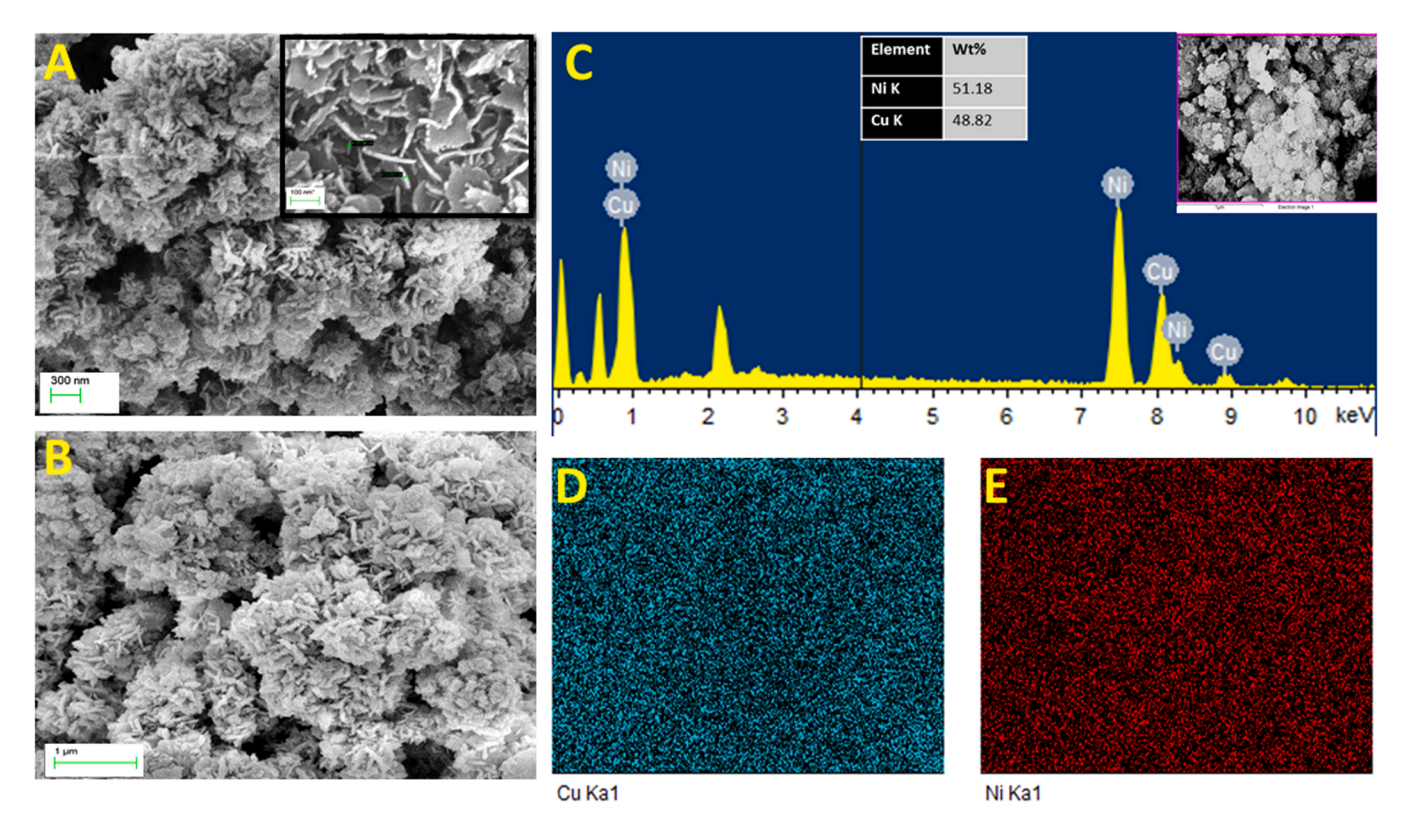


Fig. 3. SEM images of CuN-11 nanoflower at (A) 300 nm (in inset magnified image of flakes scale at 100 nm) and (B) 1 μm. (C) EDX pattern of CuNi-11 nanocatalyst, (D) elemental mapping of copper, and (E) nickel element.

of β -Ni(OH)₂, and (200) plane of copper metal nanocatalysts (Fig. 4C) [57]. The d–spacing of the planes matched well with PXRD data peaks (Fig. 1). Further, the SAED pattern showed the concentric rings which confirmed the crystalline nature of CuNi-11 nanocatalyst (Fig. 4D).

Furthermore, magnetic study of CuNi-11 nanocatalyst was performed using a vibrating-sample magnetometer (VSM), confirming the ferromagnetic nature of CuNi-11 (Figure S3) [58]. Magnetic properties of CuNi-11 were studied at room temperature with an applied field of ± 20.0 kOe. The values of saturation magnetization ($M_{\rm S}$), remanence ($M_{\rm r}$), remanence to saturation ratio ($M_{\rm r}/M_{\rm S}$), and coercivity (Hc) were calculated from the obtained M-H loop curve. These values were found to be 10.27 emu/g, 1.30 emu/g, 0.13, 75.48 Oe for $M_{\rm S}$, $M_{\rm r}$, $M_{\rm r}/M_{\rm S}$, and $H_{\rm c}$, respectively. Overall, these results highlight the ferromagnetic nature of bimetallic CuNi-11 nanocatalyst [42,58].

Finally, X-ray photoelectron spectroscopy (XPS) analysis was performed to confirm the chemical composition and the oxidation state of the catalyst (Fig. 5). The survey scan confirmed the presence of Cu, Ni, and O elements (Figure S4). The XPS spectra of Cu 2p exhibited two broad peaks of Cu $2p_{3/2}$ and Cu $2p_{1/2}$ at 933.6 eV and 953.6 eV, respectively, for the presence of CuO (i.e. Cu²⁺) as a result of surface oxidation of metallic copper (Fig. 5A) [59,60]. On the other hand, the XPS spectra of Ni 2p exhibited two peaks of Ni $2p_{3/2}$ and Ni $2p_{1/2}$ (Fig. 5B). The peak at 855.7 eV and the satellite peak at 861.2 eV for Ni $2p_{3/2}$ and at 873.3 eV and its satellite peak at 879.9 eV for Ni $2p_{1/2}$ for Ni^{+2} of $Ni(OH)_2$ [61,62]. The peak separation of 17.6 eV in Ni 2p_{3/2} and Ni 2p_{1/2} confirmed the formation of Ni(OH)₂ due to the spin-orbit coupling phenomenon [63-65]. Moreover, the O 1s peak observed at 531.2 eV confirmed the presence of hydroxide which supports the formation of nickel hydroxide in CuNi-11 nanocatalyst as shown in Fig. 5 (C) [66,67]. Furthermore, the XPS spectra of recovered catalyst were also performed, confirming the reduction of CuNi-11 nanocatalyst to Cu (0)/Ni(0) in presence of HCOOH (Figure S5(A-C)). The XPS spectra of copper Cu $2p_{3/2}$ and Cu $2p_{1/2}$ present at 932.7 eV and 953.2 eV for the formation of Cu(0) [68,69]. Additionally, the XPS spectra of Ni 2p_{3/2}

and Ni $2p_{1/2}$ observed at 852.1 eV and their satellite peaks shown in Figure S5(B) confirmed the presence of Ni metallic character [70,71]. This is an important observation since the alloy Cu(0)/Ni(0) appears to be the active catalyst form during catalytic operation.

Catalytic reaction and performance

The catalytic carboxylation reaction of different substituted benzenes using the CuNi-11 nanocatalyst in the presence of formic acid as carboxylating agent and solvent-free conditions has been performed, as shown in Scheme 2.

Initially, several catalysts including monometallic Cu and Ni, CuCl, CuNi-11, CuNi-12, and CuNi-21 were screened for the direct carboxylation of benzene using 12 mmol of formic acid for 20 hours at 55°C temperature (Fig. 6). Based on previous reports [72,73], the concept of a Lewis-acid mediated pathway was also explored by using CuCl which provided only 9% conversion and ruled out the possibility of that pathway. The reaction with monometallic Cu, monometallic Ni, CuNi-12, and CuNi-21 revealed that excess Cu and/or Ni suppress the catalytic activity, whereas an equimolar ratio of Cu and Ni species is essential for enhanced catalytic performance [74]. The synergistic effect between Cu and Ni metals enhances the catalytic activity and provides 100% conversion for the carboxylation reaction, whereas monometallic Cu and Ni alloys shows only 41% and 68% conversion of benzene into benzoic acid. The best result was obtained with CuNi-11 nanocatalyst with 100% conversion and 100% selectivity. The obtained data indicate the importance of bimetallic CuNi nanocatalyst for the catalytic conversion of benzene. Therefore, all catalytic reactions were carried out with CuNi-11 nanocatalyst.

The systematic investigation of carboxylation reactions was performed using benzene as a model substrate to efficiently select the optimal reaction conditions (e.g. loading of solvent, concentration of formic acid and substrate, reaction time and temperature). To examine the influence of solvent (2 mL), various solvents such as 2-propanol,

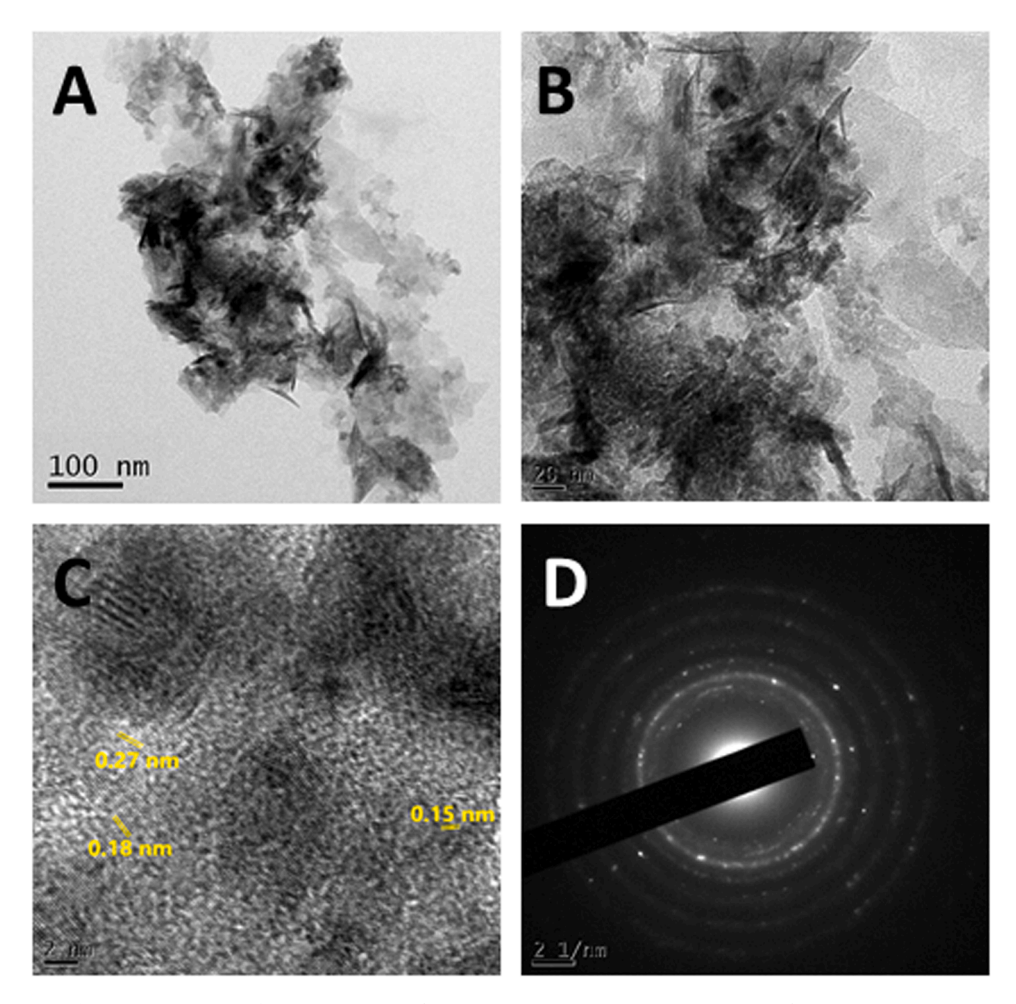


Fig. 4. TEM images of CuNi-11 nanocatalyst at (A) 100 nm (B) 20 nm (C) 2 nm and (D) SAED pattern.

methanol, water, and methanol-water mixture (1 mL each) were screened with HCOOH (12 mmol), catalyst (15 mg) for 20 hours. Remarkably, the highest conversion was obtained when the reaction was solvated with either water (100% conversion) or a water-methanol mixture (95% conversion) (Table 1). Surprisingly, a solvent-free carboxylation reaction also resulted in a maximum 100% benzene conversion and 100% selectivity to benzoic acid. Consequently, the solvent-free reaction was preferred to avoid the post-work-up process of the reaction mixture [39,75]. It is to be noted that formic acid may play the role of the solvent medium in the reaction mixture as all reagents were present in the liquid form.

Furthermore, the reaction in solvent-free conditions was carried out by varying the formic acid amount between 5 to 15 mmol, with benzene (1 mmol) and CuNi-11 (15 mg) for 20 hours. It was observed that the conversion of benzene depends significantly on the amount of HCOOH, as shown in Table 2. As the formic acid amount decreases, the conversion of benzene decreases. Specifically, 5 mmol of formic acid resulted in zero conversion, whereas 100% conversion was observed with 12 and 15 mmol of formic acid. Hence, all the reactions were carried out with 12 mmol of formic acid.

Thereafter, the effect of benzene concentration (1-2.5 mmol) was carried out with HCOOH (12 mmol), CuNi-11 (15 mg) for 20 hours at 55° C. A complete 100% conversion of benzene to benzoic acid was obtained using 1 mmol of benzene (Table 3). These results showed that as the substrate amount increases, the conversion decreases.

Moreover, a control experiment without catalyst resulted in only 17% conversion, whereas 100% conversion was obtained when 15 mg of CuNi-11 nanocatalyst was utilized (Table 4). This result showed the importance of the synthesized bimetallic CuNi-11 catalyst for the

carboxylation of benzene to benzoic acid.

The influence of temperature was studied on the carboxylation reaction. When the reaction was carried out at either room temperature and 40°C for 20 h, benzene conversion was 12% and 72%, respectively. A maximum 100% conversion with 100% selectivity was obtained at 55°C in 20 hours (Fig. 7). Hence, the final optimized reaction conditions for carboxylation of benzene were 1 mmol of benzene, 12 mmol of HCOOH, and 15 mg of CuNi-11 catalyst along with a reaction temperature of 55°C and reaction time of 20 hours to achieve complete benzene conversion and selectivity.

Furthermore, to check the applicability of the reaction, carboxylation of some simple substituted arenes including toluene, haloarenes (-Br, -Cl, -F), phenol, aniline, naphthalene, and pyridine were explored under the identified optimized reaction conditions (Table 5, Entry 1-9). Additionally, the reaction is also applicable to solid arenes such as naphthalene, using methanol as solvent (2 mL), which requires a longer reaction time to achieve 100% conversion and 100% selectivity (Table 5, Entry 5). All products and conversions were confirmed by Shimadzu GC-MS and NMR analysis (Figures S6 and S7). The kinetic study of the carboxylation reaction was performed using benzene as a model substrate by taking samples periodically at 4, 10, 15, and 20 hours and around 17, 47, 76, and 100% conversion was observed (Fig. 8A). Furthermore, the recyclability of the catalyst has been studied with model substrate benzene. After each run, the reaction mixture was separated with a magnet, then washed and dried overnight at room temperature. The recycled catalyst was reused for up to six consecutive cycles (Fig. 8B).

To check the leaching of the catalyst, a hot-filtration test was performed [4,76]. The reaction was stirred for 4 hours, and the catalyst was

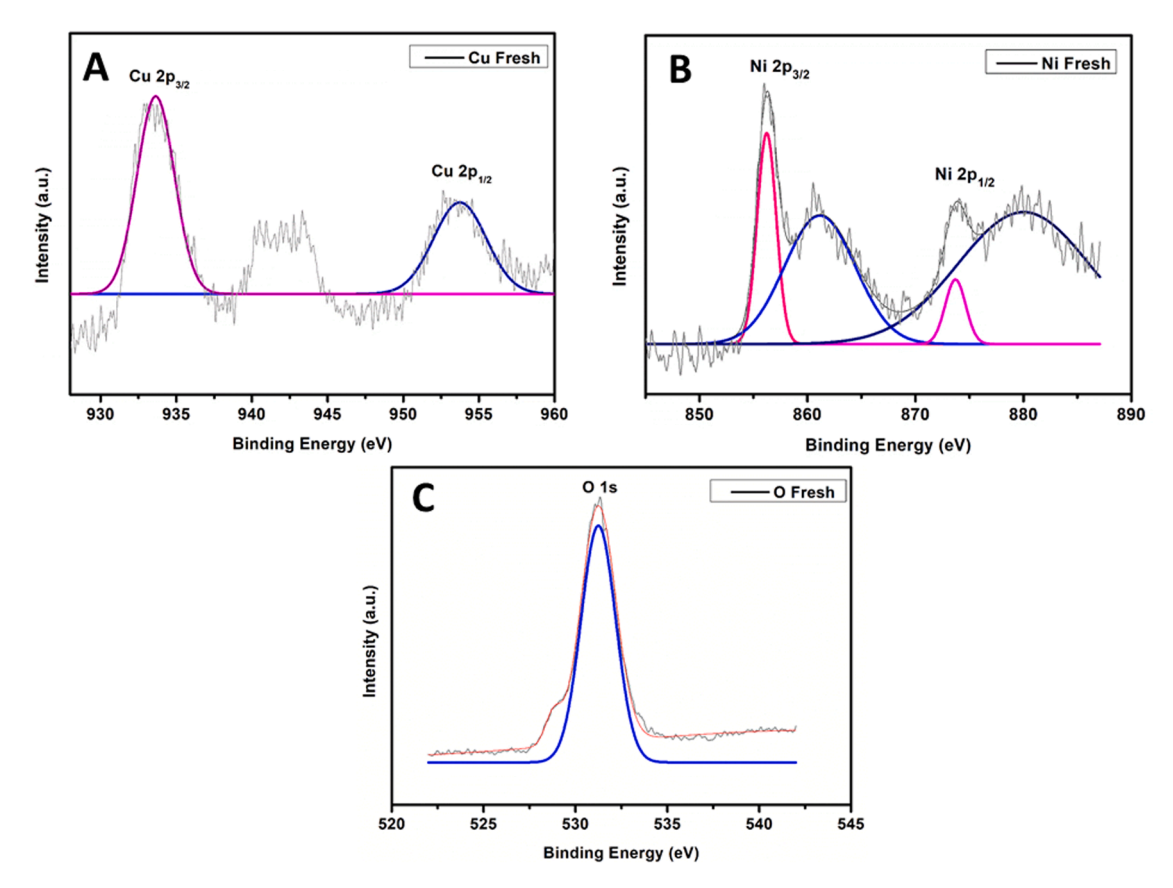
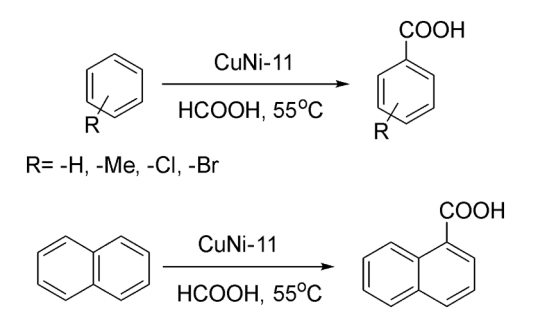


Fig. 5. XPS spectra of (A) Cu 2p (B) Ni 2p and (C) O 1s of synthesized CuNi-11 nanocatalyst.



Scheme 2. Catalytic conversion reaction scheme of substituted benzene to corresponding benzoic acids using CuNi-11 nanocatalyst.

CATALYST OPTIMIZATION

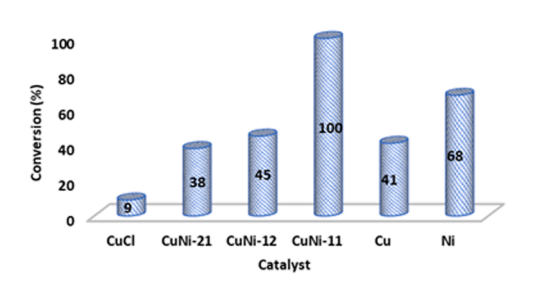


Fig. 6. Effect of different catalysts on the conversion of benzene to benzoic acid. Reaction conditions: Benzene (1 mmol), Catalyst (15 mg), HCOOH (12 mmol), Time (20 h), Temperature (55° C).

Table 1
Effect of solvent on the conversion of benzene into benzoic acid

Entry	Solvent(2 mL)	CuNi-11(mg)	Formic acid(mmol)	Conversion(%)
1	H ₂ O	15	15	100
2	MeOH	15	15	71
3	H ₂ O:MeOH	15	15	95
4	2-Propanol	15	15	47
5	-	15	15	100

Reaction conditions: Substrate (benzene) = 1 mmol, Catalyst (CuNi-11) = 15 mg, Formic acid = 15 mmol, Solvent = 2 mL, Time = 20 h, Temperature = 55° C.

 Table 2

 Effect of amount of formic acid on carboxylation of benzene

Entry	Formic acid(mmol)	CuNi-11(mg)	Conversion(%)	
1	5	15	-	
2	8	15	17	
3	10	15	77	
4	12	15	100	
5	15	15	100	

Reaction conditions: Substrate (benzene) = 1 mmol, Catalyst (CuNi-11) = 15 mg, Formic acid =5-15 mmol, Time = 20 h, Temperature = 55° C.

separated with a magnet. Then, the reaction mixture was filtered using filter paper. Further, the supernatant was proceeded and stirred as a reaction mixture to react without catalyst and the sample was taken for GC-MS analysis. There was no conversion observed after catalyst removal, indicating no leaching of the Cu and Ni metals. Also, the supernatant was characterized via ICP-OES and the analysis reveals no significant leaching of Cu and Ni metals (Table S1).

Further, to check the morphological changes in the recovered catalyst, FE-SEM was performed in which no significant changes were

Table 3Effect of substrate amount on carboxylation reaction of benzene

Entry	Substrate(mmol)	Formic acid(mmol)	Conversion(%)
1	1	12	100
2	1.5	12	47
3	2	12	33
4	2.5	12	15

Reaction conditions: Substrate (benzene) = 1-2.5 mmol, Catalyst (CuNi-11) = 15 mg, Formic acid = 12 mmol, Time = 20 h, Temperature = 55°C.

Table 4Effect of catalyst amount loading on carboxylation of benzene

Entry CuNi-11(mg)		Formic acid(mmol)	Conversion(%)	
1	-	12	17	
2	3	12	36	
3	6	12	47	
4	9	12	58	
5	12	12	80	
6	15	12	100	

Reaction conditions: Substrate (benzene) = 1 mmol, Catalyst (CuNi-11) = 0-15 mg, Formic acid = 12 mmol, Time = 20 h, Temperature = 55° C.

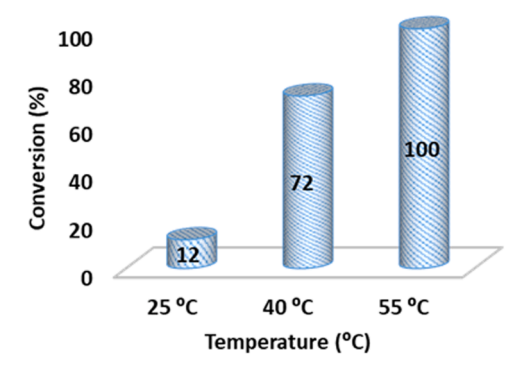


Fig. 7. Effect of temperature on the carboxylation reaction of benzene. Reaction conditions: Benzene (1 mmol), Catalyst CuNi-11 (15 mg), Formic acid (12 mmol), Temperature (25-55°C), Time (20 hours).

observed in the structure of the recovered catalyst (Figure S8). These results reveal that the synthesized catalyst is recyclable, reusable, and robust in nature. Additionally, to get more evidence of the formation of benzoic acid, Fourier transformation infrared spectroscopy (FT-IR) was performed on the isolated product. The analysis showed absorbance peaks at 3073, 2827, 1682, 1288, and 933 cm $^{-1}$ for O-H, C-H, C=O and aryl C-H vibrations of benzoic acid (Figure S9) [77,78]. Furthermore, an isotopic-labelling experiment was performed under standard reaction conditions using C_6D_6 as substrate and formic acid as carboxylating agent, and the corresponding expected deuterated acidic product was obtained (Figure S10).

To the best of our knowledge, the mechanistic aspects of the direct carboxylation of benzene with formic acid on CuNi-11 bimetallic catalyst remain unknown. In this regard, we performed DFT calculations to gain valuable insights into the potential reaction mechanism. We considered the alloy Cu(0)/Ni(0) form of the catalyst as suggested by the XPS analysis of recovered catalyst (Figure S5). Scheme 3 presents a proposed reaction mechanism for the carboxylation of benzene to benzoic acid with formic acid as carboxylating agent on the CuNi-11 nanocatalyst surface. The computed reaction energy profile and graphical snapshots of relevant reactants, intermediates, and transition states (TSs) for the reaction on (111) CuNi-11 surface are shown in Fig. 9. Importantly, our PXRD analysis has authenticated the active sites of CuNi-11 nanocatalyst are located on the (111) plane surface, as depicted in Fig. 1.

In the first step of the cycle, benzene chemisorbs through its π electron cloud with hexagonal close-packed (hcp) flat-lying orientation, involving the H-flipped configuration of the ring [79]. Generally, it is established that benzene adsorbs on transition metals with its aromatic ring lying parallel to the surface [80-83], similar to the adsorption of biomass derived rings on metal catalysts [84]. The computed binding energy of benzene on (111) of CuNi-11 three-fold hollow site is -137.7 kJ mol⁻¹, whereas DFT-computed adsorption energy of benzene ranges between -54.0 to -103.2 and -84.0 to -101.3 kJ mol⁻¹ on three-fold hollow sites of (111) Cu [85-87] and Ni [80,88-90] metals, respectively. The stronger binding energy of benzene on CuNi-11 catalyst relative to Cu and Ni metals may be traced down to (i) a larger overlap of benzene π orbitals with the orbitals of the CuNi-11 surface than that with either Cu or Ni surface individually and (ii) better description of adsorbate-surface dispersion interactions by PBE-D3 method (see computational methods in supporting information). At the hcp adsorbed state (C₆H₆*), the mechanism is initiated by activation of benzene C-H bond and formation of tilted phenyl (C₆H₅*) intermediate with a neighboring H'* species occupying the hcp site. The geometry structure for benzene C-H scission TS (TS1) exhibits the breaking of a σ bond, featuring a three-membered metallacycle C-Cu-H, with an activation energy barrier of 180.9 kJ mol⁻¹. Formic acid then adsorbs nearly perpendicular with its carbonyl oxygen bonded atop on a Ni site and C-H bond pointing towards a bridge Cu-Ni site. The computed adsorption energy of formic acid is -60.1 kJ mol⁻¹, indicating an energetically favorable process. Several theoretical studies have investigated formic acid adsorption and decomposition on Cu and Ni (111) surfaces and reported atop adsorption through the carbonyl oxygen, with binding energies of -46.3 and -34.7 kJ mol⁻¹ for Cu and Ni metals, respectively [30,91,92]. After adsorption, formic acid decomposes into adsorbed bidentate carboxyl intermediate (COOH*) and atomic hcp-bounded H"*. Furthermore, breaking the C-H bond in HCOOH (TS2) on CuNi bimetallic surface is exothermic (-65.4 kJ mol⁻¹), with an activation barrier of 46.3 kJ mol⁻¹. Jiang and coworkers investigated the activation of the HCOOH C-H bond on the Cu (111) surface and reported an activation energy barrier of 36.7 kJ mol⁻¹ [35]. Dehydrogenation of HCOOH to the formate intermediate (HCOO*) [93] via the cleavage of the O-H bond, followed by C-H bond scission to produce CO2* and 2H* was not considered herein, as the liberation of CO2 gas was not detected experimentally via lime water test. In the next step, the surface-bound hydrogens on adjacent hcp sites (H'* + H''*) recombine to form molecular hydrogen. The H-H bond formation (TS3) takes place on top of a Ni atom, with an activation barrier of 74.4 kJ mol⁻¹. The atop adsorbed molecular hydrogen desorbs from the surface with an energetic penalty of 53.1 kJ mol⁻¹. Liberation of H₂ gas was detected by the flame test, supporting the proposed reaction mechanism. Lastly, C7H6O2 forms on the hcp site through the recombination of phenyl and carboxyl intermediates via TS4. The recombination step is exothermic with reaction and activation energy barriers of 80.7 and 36.2 kJ mol⁻¹, respectively.

The catalytic cycle completes with benzoic acid desorbing to regenerate the catalyst, with desorption energy of 137.6 kJ mol⁻¹. Overall, benzene C-H bond activation was found to be the rate-determining step in the carboxylation reaction. Finally, to demonstrate the solvation effects on the reaction mechanism, the self-consistent continuum solvation model was applied on the DFT optimized structures, as shown in Figure S11, by utilizing both formic acid and benzene as the solvation medium for the reaction [94]. We showed that implicit solvation effects do not change the reaction pathway energetics.

Conclusions

In summary, we utilize synthesis, characterization and catalytic experiments together with first principles calculations to report the first example of direct carboxylation of benzene on bimetallic CuNi-11 nanocatalyst. The reaction proceeds through the activation of both benzene and formic acid with desorption of molecular H_2 . The CuNi-11

Table 5Carboxylation of selected substituted arenes into their corresponding acids.

Entry	Substrate	Product	Time (hr)	Conversion (%)	Selectivity (%)
1		СООН	20	100	100
2		СООН	30	100	100
3	Br	СООН	31	100	100
4		Вг СООН	31	100	100
5	CI	СООН	30	100	100
6	F H ₂ N	СООН	29	100	100
7	HO	H ₂ N COOH	35	100	100
8	HO N	COOH	28	100	100
9 ^a	IN CONTRACTOR OF THE PROPERTY	СООН	40	100	100

Reaction conditions: Substrate = 1 mmol, Catalyst (CuNi-11) = 15 mg (0.0096 mol%), Formic acid = 12 mmol, Time = 20-40 h, Temperature $= 55^{\circ}$ C.

^a Methanol used as solvent due to solubility issue in water.

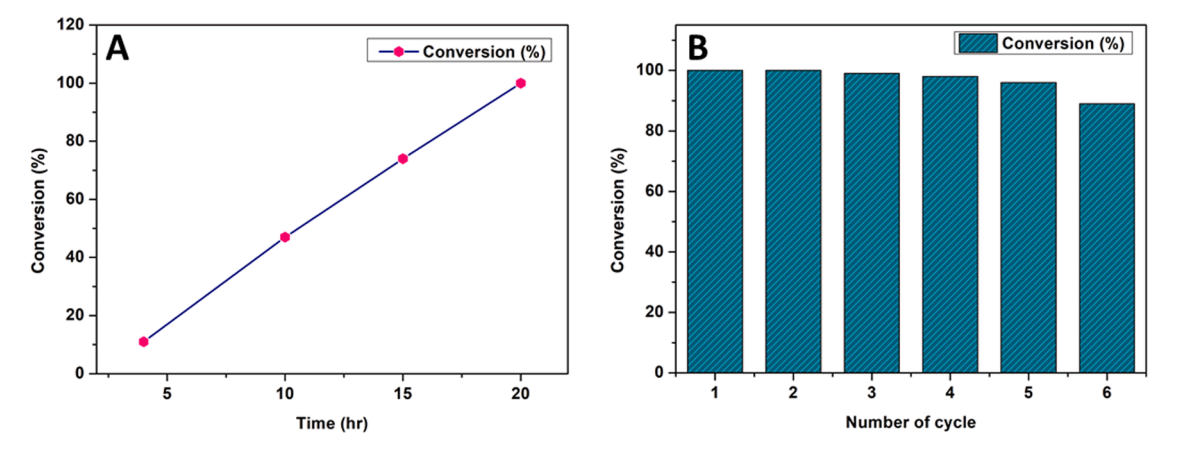
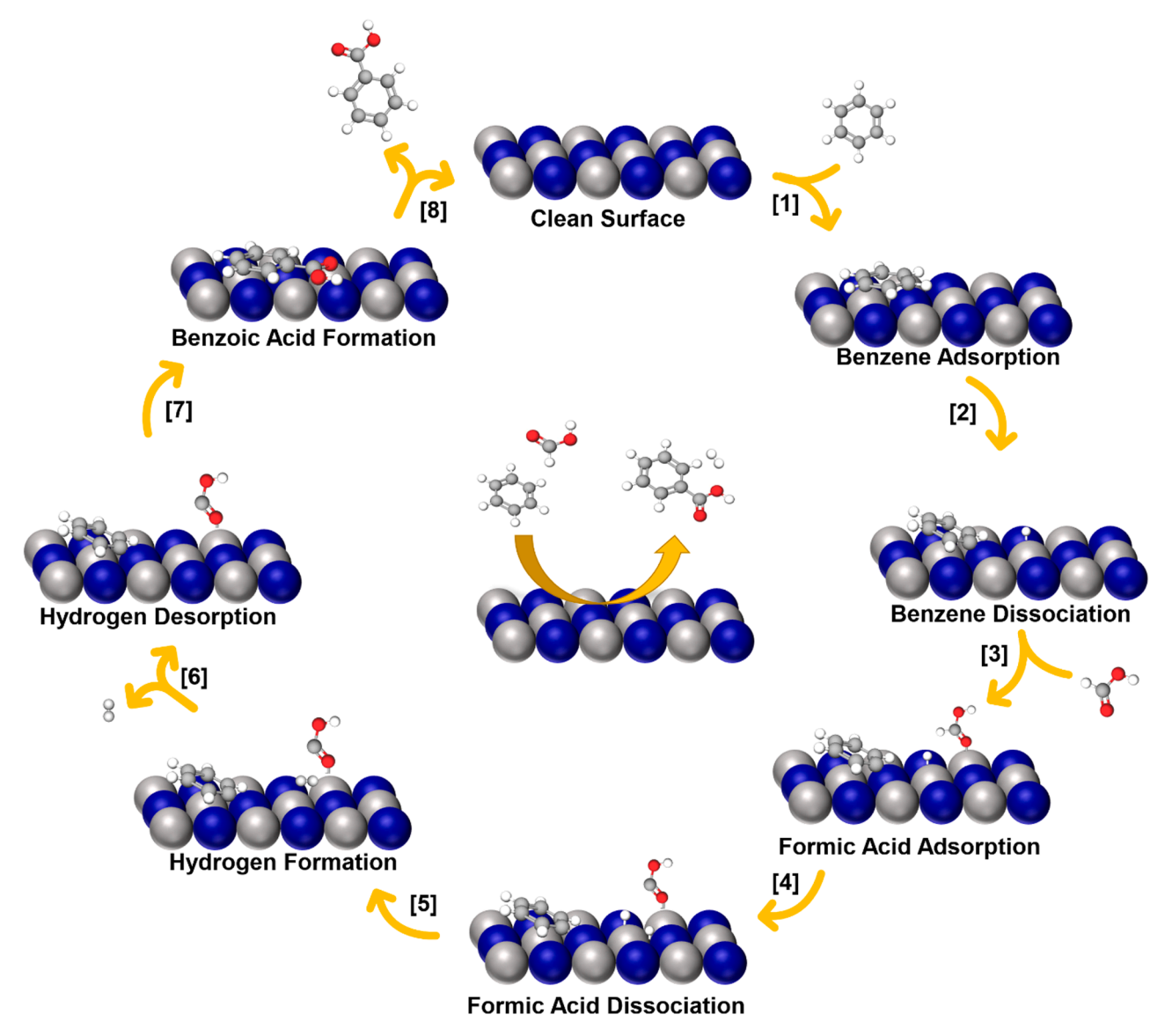


Fig. 8. (A) Kinetic study and (B) Catalyst reusability of the carboxylation reaction of benzene for all the cyclic runs. Reaction conditions: Substrate (benzene) = 1 mmol, Catalyst (CuNi-11) = 15 mg, Formic acid = 12 mmol, Time = 4-20 h, Temperature = 55° C.

nanocatalyst is highly efficient, recyclable, and cost-effective. Our work advances the field of arene functionalization by introducing an activator-, additive- and solvent-free carboxylation reaction at mild conditions using a recyclable bimetallic CuNi-11 catalyst, while providing a

mechanistic understanding of the reaction.



Scheme 3. Plausible mechanism of benzene carboxylation with formic acid on bimetallic nanoparticles.

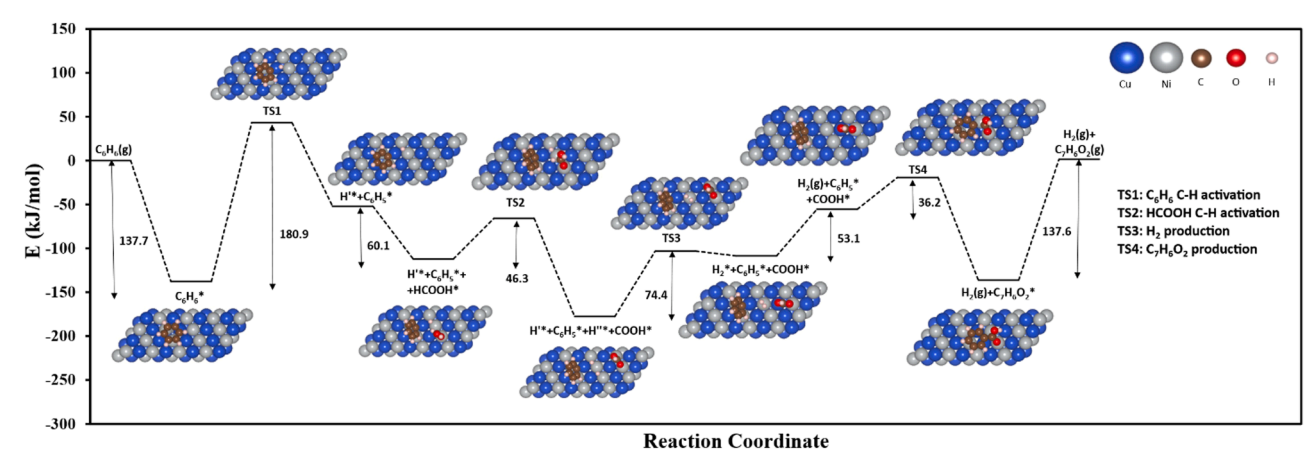


Fig. 9. Potential energy surface of direct carboxylation of benzene to benzoic acid on close-packed fcc (111) CuNi-11 bimetallic surface. The detailed structures of reactants, transition states, intermediates, and products are schematically illustrated in insets.

CRediT authorship contribution statement

Neha Choudhary: Methodology, Writing – original draft. Mona Abdelgaid: Software, Formal analysis, Writing – original draft. Giannis Mpourmpakis: Supervision, Conceptualization, Writing – review & editing. Shaikh M. Mobin: Conceptualization, Supervision, Writing – review & editing.

Declaration of Competing Interest

There are no conflicts to declare.

Data availability

Data will be made available on request.

Acknowledgments

S.M.M. thanks SERB-DST, New Delhi, India (Project CRG/ 2020/ 001769), BRNS, Mumbai, India (Project 58/14/17/2020- BRNS/ 37215), and IIT Indore for financial support. N.C. thanks to UGC, New Delhi for fellowship. We are also thankful to sophisticated instrumentation centre (SIC), IIT-Indore for providing the characterization facilities. We would also like to acknowledge SAIF, IIT-Bombay for HR-TEM analysis, IIT-GN for ICP-OES analysis and MRC at MNIT-Jaipur for XPS, IIC at IIT-Roorkee for VSM and SEM-EDAX, Mapping analysis. Also we would like to thank MEMS Department, IIT-Indore for FT-IR analysis. G. M. and M.A. acknowledge support by the National Science Foundation (NSF), under grant no. 1920623. Computational support has been provided by the Center for Research Computing at the University of Pittsburgh and the Extreme Science and Engineering Discovery Environment (XSEDE), which is supported by NSF (ACI-1548562).

Supplementary materials

Supplementary material associated with this article can be found, in the online version, at doi:10.1016/j.mcat.2022.112620.

References

- [1] Y. Zhang, J. Yang, R. Ge, J. Zhang, J.M. Cairney, Y. Li, M. Zhu, S. Li, W. Li, Coord. Chem. Rev. 461 (2022), 214493.
- [2] R. Narayanan, M.A. El-Sayed, J. Phys. Chem. B 109 (2005) 12663–12676.
- [3] X. Cui, W. Li, P. Ryabchuk, K. Junge, M. Beller, Nat. Catal. 1 (2018) 385-397.
- [4] M.Ali Nasseri, Z. Rezazadeh, M. Kazemnejadi, A. Allahresani, Dalton Trans 49 (2020) 10645–10660.
- [5] M.A. Nasseri, Z. Rezazadeh, M. Kazemnejadi, A. Allahresani, Catal. Lett. 151 (2021) 1049–1067.
- [6] M. Kazemnejadi, R. Omer Ahmed, B. Mahmoudi, RSC Adv 10 (2020) 43962–43974.
- [7] J. Govan, Y.K. Gun'ko, Nanomaterials 4 (2014) 222-241.
- [8] I. Mustieles Marin, J.M. Asensio, B. Chaudret, ACS Nano 15 (2021) 3550–3556.
- [9] Q. Zhang, X. Yang, J. Guan, ACS Appl. Nano Mater 2 (2019) 4681-4697.
- [10] H. Yue, C. Zhu, L. Huang, A. Dewanji, M. Rueping, Chem. Commun. 58 (2022) 171–184.
- [11] A. del Olmo, J. Calzada, M. Nuñez, Crit. Rev. Food Sci. Nutr. 57 (2017) 3084–3103.
- [12] A.N. Sarve, P.A. Ganeshpure, P. Munshi, Ind. Eng. Chem. Res. 51 (2012) 5174–5180.
- [13] C.-H. Jun, C.W. Moon, D.-Y. Lee, Chem. Eur. J. 8 (2002) 2422–2428.
- [14] J. Luo, I. Larrosa, ChemSusChem 10 (2017) 3317–3332.
- [15] L. J. L. I. Chemsuschem 10 (2017) 3317–3332.
- [16] D. Liu, Z. Xu, M. Liu, Y. Fu, Org. Chem. Front. 9 (2022) 370–379.
- [17] A. Correa, R. Martín, J. Am. Chem. Soc. 131 (2009) 15974–15975.
- [18] S. Wang, G. Du, C. Xi, Org. Biomol. Chem. 14 (2016) 3666–3676.
 [19] C. Pei, J. Zong, S. Han, B. Li, B. Wang, Org. Lett. 22 (2020) 6897–6902.
- [20] A. Gevorgyan, K.H. Hopmann, A. Bayer, Chem. Eur. J. 26 (2020) 6064–6069.
- [21] T. Suga, H. Mizuno, J. Takaya, N. Iwasawa, Chem. Commun. 50 (2014) 14360–14363.
- [22] F.-P. Wu, J.-B. Peng, X. Qi, X.-F. Wu, J. Org. Chem. 82 (2017) 9710-9714.
- [23] M.G. Mura, L.D. Luca, G. Giacomelli, A. Porcheddu, Adv. Synth. Catal. 354 (2012) 3180–3186.

- [24] D. Mellmann, P. Sponholz, H. Junge, M. Beller, Chem. Soc. Rev. 45 (2016) 3954–3988.
- [25] X. Qi, C.-L. Li, L.-B. Jiang, W.-Q. Zhang, X.-F. Wu, Catal. Sci. Technol. 6 (2016) 3099–3107.
- [26] J. Scaranto, M. Mavrikakis, Surf. Sci. 648 (2016) 201-211.
- [27] M. Rafiee, H. Bashiri, Catal. Commun. 137 (2020), 105942.
- [28] B.W.J. Chen, S. Bhandari, M. Mavrikakis, ACS Catal 11 (2021) 4349-4361.
- [29] X. Li, K. Xuan, Y. Zhu, G. Chen, G. Yang, Appl. Surf. Sci. 452 (2018) 87–95.
- [30] Q. Luo, G. Feng, M. Beller, H. Jiao, J. Phys. Chem. C 116 (2012) 4149–4156.
- [31] B.W.J. Chen, M. Stamatakis, M. Mavrikakis, ACS Catal 9 (2019) 9446–9457.
- [32] S. Singh, S. Li, R. Carrasquillo-Flores, A.C. Alba-Rubio, J.A. Dumesic, M. Mavrikakis, AIChE J. 60 (2014) 1303–1319.
- [33] Y.-Y. Wang, Prog. React. Kinet. Mech. 44 (2019) 67-73.
- [34] Z. Jiang, N. Ye, T. Fang, Chem. Phys. Lett. 751 (2020), 137509.
- [35] F. He, K. Li, G. Xie, Y. Wang, M. Jiao, H. Tang, Z. Wu, J. Power Sources 316 (2016) 8–16.
- [36] D. Wang, D. Astruc, Chem. Soc. Rev. 46 (2017) 816-854.
- [37] H. Takeda, C. Cometto, O. Ishitani, M. Robert, ACS Catal 7 (2017) 70-88.
- [38] K. Tanaka, F. Toda, Chem. Rev. 100 (2000) 1025-1074.
- [39] S. Ni, M. Hribersek, S.K. Baddigam, F.J.L. Ingner, A. Orthaber, P.J. Gates, L. T. Pilarski, Angew. Chem. Int. Ed. 60 (2021) 6660–6666.
- [40] D.S. Hall, D.J. Lockwood, C. Bock, B.R. MacDougall, Proc. R. Soc. Math. Phys. Eng. Sci. (2022).
- [41] J.A. Witt, D.R. Mumm, A. Mohraz, J. Mater. Chem. A 4 (2016) 1000-1007.
- [42] M. Biswas, A. Saha, M. Dule, T.K. Mandal, J. Phys. Chem. C 118 (2014) 22156–22165.
- [43] K. Xiao, X. Qi, Z. Bao, X. Wang, L. Zhong, K. Fang, M. Lin, Y. Sun, Catal. Sci. Technol. 3 (2013) 1591–1602.
- [44] H. Keshavarz, A. Khavandi, S. Alamolhoda, M. Reza Naimi-Jamal, RSC Adv. 10 (2020) 39008–39016.
- [45] G. Su, C. Yang, J.-J. Zhu, Langmuir 31 (2015) 817-823.
- [46] J. Ahmed, K.V. Ramanujachary, S.E. Lofland, A. Furiato, G. Gupta, S. M. Shivaprasad, A.K. Ganguli, Colloids Surf. Physicochem. Eng. Asp. 331 (2008) 206–212
- [47] P.H.K. Charan, G. Ranga Rao, Microporous Mesoporous Mater 200 (2014) 101–109.
- [48] N. Choudhary, T. Ghosh, S.M. Mobin, Chem. Asian J. 15 (2020) 1339-1348.
- [49] K.S.W. Sing, Pure Appl. Chem. 57 (1985) 603-619.
- [50] G. Mayakrishnan, V. Elayappan, I.S. Kim, I.-M. Chung, Sci. Rep. 10 (2020) 1-15.
- [51] S.N. Ansari, P. Kumar, A.K. Gupta, P. Mathur, S.M. Mobin, Inorg. Chem. 58 (2019) 9723–9732.
- [52] N. Austin, B. Butina, G. Mpourmpakis, Prog. Nat. Sci. Mater. Int. 26 (2016) 487–492.
- [53] R. Cheula, M. Maestri, G. Mpourmpakis, ACS Catal 10 (2020) 6149-6158.
- [54] Y. Luo, L. Tang, U. Khan, Q. Yu, H.-M. Cheng, X. Zou, B. Liu, Nat. Commun. 10 (2019) 269.
- [55] B. Deka Boruah, A. Misra, ACS Appl. Mater. Interfaces 8 (2016) 18182–18188.
- [56] X. Xiao, D. Huang, Y. Fu, M. Wen, X. Jiang, X. Lv, M. Li, L. Gao, S. Liu, M. Wang, C. Zhao, Y. Shen, ACS Appl. Mater. Interfaces 10 (2018) 4689–4696.
- [57] G.-X. Tong, F.-T. Liu, W.-H. Wu, J.-P. Shen, X. Hu, Y. Liang, CrystEngComm 14 (2012) 5963–5973.
- [58] M. Raula, Md.H. Rashid, S. Lai, M. Roy, T.K. Mandal, ACS Appl. Mater. Interfaces 4 (2012) 878–889.
- [59] C.-K. Wu, M. Yin, S. O'Brien, J.T. Koberstein, Chem. Mater. 18 (2006) 6054–6058.
- [60] S.D. Jones, L.M. Neal, H.E. Hagelin-Weaver, Appl. Catal. B Environ. 84 (2008) 631–642.
- [61] S.-Q. Liu, H.-R. Wen, Y.-W.Zhu Ying-Guo, X.-Z. Fu, R. Sun, C.-P. Wong, Nano Energy 44 (2018) 7–14.
- [62] M. Chhetri, S. Sultan, C.N.R. Rao, Proc. Natl. Acad. Sci 114 (2017) 8986–8990.
- [63] S. Anantharaj, P.E. Karthik, S. Kundu, Catal. Sci. Technol. 7 (2017) 882–893.
- [64] N. Weidler, J. Schuch, F. Knaus, P. Stenner, S. Hoch, A. Maljusch, R. Schäfer, B. Kaiser, W. Jaegermann, J. Phys. Chem. C 121 (2017) 6455–6463.
- [65] L.M. Vicente-Arche, J. Bréhin, S. Varotto, M. Cosset-Cheneau, S. Mallik, R. Salazar, P. Noël, D.C. Vaz, F. Trier, S. Bhattacharya, A. Sander, P.L. Fèvre, F. Bertran, G. Saiz, G. Ménard, N. Bergeal, A. Barthélémy, H. Li, C.-C. Lin, D.E. Nikonov, I. A. Young, J.E. Rault, L. Vila, J.-P. Attané, M. Bibes, Adv. Mater. (2022), 2102102 n/a.
- [66] S. Dutta, A. Indra, Y. Feng, T. Song, U. Paik, ACS Appl. Mater. Interfaces 9 (2017) 33766–33774.
- [67] Y.-Z. Su, K. Xiao, N. Li, Z.-Q. Liu, S.-Z. Qiao, J. Mater. Chem. A 2 (2014) 13845–13853.
- [68] Y. Yu, R. Jin, J. Easa, W. Lu, M. Yang, X. Liu, Y. Xing, Z. Shi, Chem. Commun. 55 (2019) 4178–4181.
- [69] M. Li, F. Cárdenas-Lizana, M.A. Keane, Appl. Catal. Gen. 557 (2018) 145–153.
- [70] E.L. Ratcliff, J. Meyer, K.X. Steirer, A. Garcia, J.J. Berry, D.S. Ginley, D.C. Olson, A. Kahn, N.R. Armstrong, Chem. Mater. 23 (2011) 4988–5000.
- [71] O.U. Valdés-Martínez, C.E. Santolalla-Vargas, V. Santes, J.A. de los Reyes, B. Pawelec, J.L.G. Fierro, Catal. Today 329 (2019) 149–155.
- [72] Y. Suzuki, T. Hattori, T. Okuzawa, S. Miyano, Chem. Lett. 31 (2002) 102–103.
- [73] G.A. Olah, B. Török, J.P. Joschek, I. Bucsi, P.M. Esteves, G. Rasul, G.K. Surya Prakash, J. Am. Chem. Soc. 124 (2002) 11379–11391.
- [74] Y. Fujiwara, K. Tabaki, Y. Taniguchi, Synlett 1996 (1996) 591–599.
- [75] D. Fildes, V. Caignaert, D. Villemin, P.-A. Jaffrès, Green Chem 3 (2001) 52–56.
- [76] H. Gruber-Woelfler, P.F. Radaschitz, P.W. Feenstra, W. Haas, J.G. Khinast, J. Catal. 286 (2012) 30–40.

- [77] W.A. Rodríguez-Rodríguez, J. Colón, R. Guzmán, H. Rivera, M.B. Santiago-Berríos, Mater. Res. Express 1 (2014), 035906.
- [78] G.B. Tolstorozhev, M.V. Bel'kov, I.V. Skornyakov, O.K. Bazyl, V. Ya. Artyukhov, G. V. Mayer, O.I. Shadyro, P.V. Kuzovkov, S.D. Brinkevich, S.N. Samovich, J. Appl. Spectrosc. 81 (2014) 109–117.
- [79] A. Bilić, J.R. Reimers, N.S. Hush, R.C. Hoft, M.J. Ford, J. Chem. Theory Comput. 2 (2006) 1093–1105.
- [80] S.J. Carey, W. Zhao, C.T. Campbell, Surf. Sci. 676 (2018) 9-16.
- [81] M. Saeys, M.-F. Reyniers, G.B. Marin, M. Neurock, J. Phys. Chem. B 106 (2002) 7489–7498.
- [82] C. Morin, D. Simon, P. Sautet, J. Phys. Chem. B 108 (2004) 5653-5665.
- [83] M. Sacchi, P. Singh, D.M. Chisnall, D.J. Ward, A.P. Jardine, W. Allison, J. Ellis, H. Hedgeland, Faraday Discuss 204 (2017) 471–485.
- [84] V. Vorotnikov, G. Mpourmpakis, D.G. Vlachos, ACS Catal 2 (2012) 2496-2504.
- [85] J.-H. Choi, Z. Li, P. Cui, X. Fan, H. Zhang, C. Zeng, Z. Zhang, Sci. Rep. 3 (2013) 1925.

- [86] W. Liu, V.G. Ruiz, G.-X. Zhang, B. Santra, X. Ren, M. Scheffler, A. Tkatchenko, New J. Phys. 15 (2013), 053046.
- [87] T.W. White, N. Martsinovich, A. Troisi, G. Costantini, J. Phys. Chem. C 122 (2018) 17954–17962.
- [88] A.K. Myers, G.R. Schoofs, J.B. Benziger, J. Phys. Chem. 91 (1987) 2230–2232, https://doi.org/10.1021/j100293a002.
- [89] L. Delle Site, A. Alavi, C.F. Abrams, Phys. Rev. B 67 (2003), 193406.
- [90] F. Mittendorfer, J. Hafner, Surf. Sci. 472 (2001) 133-153.
- [91] Z. Jiang, P. Qin, T. Fang, Appl. Surf. Sci. 396 (2017) 857-864.
- [92] J.A. Herron, J. Scaranto, P. Ferrin, S. Li, M. Mavrikakis, ACS Catal 4 (2014) 4434–4445.
- [93] T.C. Lin, U. De La Torre, A. Hejazi, S. Kwon, E. Iglesia, J. Catal. 404 (2021) 814–831.
- [94] O. Andreussi, I. Dabo, N. Marzari, J. Chem. Phys. 136 (2012), 064102.